$LaSeTe_2$—Temperature Dependent Structure Investigation and Electron Holography on a Charge-Density-Wave-Hosting Compound

Thomas Doert,*[a] Boniface Polequin Tsinde Fokwa,[a] Paul Simon,[b] Sven Lidin,[c] and Tilo Söhnel[a]

Dedicated to Professor Peter Böttcher

Abstract: Single crystals of $LaSeTe_2$ have been prepared by reaction of the elements in a LiCl/RbCl flux at 970 K for seven days. Satellite reflections observed in diffraction experiments indicate the presence of an incommensurate lattice distortion, which is of the charge-density-wave (CDW) type. The modulated structure has been solved from X-ray data at 173, 293, and 373 K. $LaSeTe_2$ crystallizes in the 3+1-dimensional orthorhombic superspace group $Cmcm(00\gamma)s00$ (No. 63.2) with lattice parameters of $a=4.295(1)$, $b=25.371(4)$, $c=4.306(1)$ Å (173 K), $a=4.297(1)$, $b=25.408(4)$, $c=4.309(1)$ Å (293 K), and $a=4.309(1)$, $b=25.481(6)$, $c=4.321(1)$ Å (373 K). The modulation vector $\mathbf{q}=(0, 0, 0.288)$ does not change over the temperature interval. Electron holographic investigations confirm the existence of the modulation and help to visualize the charge-density wave.

Keywords: charge-density wave · electron holography · lanthanides · polychalcogenides · solid-state structure

Introduction

Polychalcogenides are, in general, characterized by the occurrence of E–E bonds (E = S, Se, Te). Due to the formation of oligomeric or polymeric anions, these types of compounds often crystallize with low-dimensional structures that can give rise to interesting physical properties, such as charge-density waves (CDWs), anisotropic optical properties, or thermoelectricity. Especially in polytellurides, extended Te–Te bonding is frequently observed. The crystal structures of all lanthanide polytellurides $LnTe_n$ (Ln = Y, La, Ce–Lu; $n>1.5$), for example, contain one-dimensional chains or two-dimensional square nets of the anions. Depending on the electron count, these square nets are prone to distortions and many of the compounds are found to crystallize with commensurately or incommensurately modulated superstructures, rather than with a high-symmetry square arrangement of the chalcogen atoms.[1,2] The structures of the rare-earth dichalcogenides $LnE_{2-\delta}$ ($0\leq\delta<0.4$), as well as those of some related pnictides LnY_2 (Y = P, As, Sb) and pnicochalcogenides LnEY can, for example, be regarded as superstructures of the ZrSSi type (cf. e.g., ref. [2] and references cited therein).

Rare-earth tritellurides $LnTe_3$ were first described in the 1960s.[3] According to these early investigations, all of the compounds crystallize with a $NdTe_3$-type structure in space group $Cmcm$ (No. 63). The structure consists of puckered [LnTe] double slabs and square-planar [Te] layers stacked along the b axis in the order -[LnTe]-[Te]-[Te]-. A single-crystal X-ray structure determination of $SmTe_3$, confirmed the structure-type assignment.[4] However, the electron diffraction patterns of several $LnTe_3$ compounds exhibit satellite reflections due to incommensurate lattice distortions, which were described to be of the CDW type.[5] The origin of the modulation can be understood by the considerable nesting of the Fermi surface. As a consequence of the distortion, an energy gap at the Fermi surface occurs. A direct observation of this energy gap by angle-resolved photoemission spectroscopy has been reported for CDW-hosting $SmTe_3$.[6] Nevertheless, refinements of the modulated structures of the $LnTe_3$ compounds have not yet been published.

[a] Dr. T. Doert, B. P. T. Fokwa, Dr. T. Söhnel
Institute of Inorganic Chemistry
University of Technology Dresden
Mommsenstr. 13, 01062 Dresden (Germany)
Fax: (+49) 351-463-37287
E-mail: thomas.doert@chemie.tu-dresden.de

[b] Dr. P. Simon
Institute of Applied Physics and Didactic of Physics
University of Technology Dresden
Present address:
Max-Planck-Institute for Chemical Physics of Solids
01187 Dresden (Germany)

[c] Prof. Dr. S. Lidin
Institute of Inorganic Chemistry—Arrhenius Laboratory
Stockholm University, 10691 Stockholm (Sweden)

 DOI: 10.1002/chem.200305148

Recently, we reported the structure of $PrSeTe_2$, an ordered ternary rare-earth polychalcogenide adopting the $NdTe_3$ structure.[7] $PrSeTe_2$, in contrast to all binary compounds of this structure type, does not show any satellite reflections in X-ray or electron diffraction experiments at room temperature. However, for $LaSeTe_2$, a further example of this class of compounds, satellite reflections are indeed observed. The results of our investigations on this CDW compound are reported here.

Results and Discussion

HREM and electron holography: High-resolution electron microscopy (HREM) and selected area electron diffraction (SAED) are widely used in the structural investigation of solids. In both imaging techniques, however, the amplitude of the image wave, which corresponds to the intensity of the image, is transmitted, whereas the phase information is partially lost. In electron holography, both the phase and the amplitude of the image wave are transferred simultaneously. This additional information allows the visualization of phase shifts caused by the investigated object. Electron holography has, until now, mainly been used in materials science to image potential and charge distribution in ceramic or semiconducting materials, for example, charge distribution across interfaces between doped layers or across quantum well structures.[8] However, electron holography can also be used to visualize the direction and magnitude of charge-density waves, as will be demonstrated in the following.

Any modulation in $LaSeTe_2$ would be expected to occur in the [Te] net and should thus be visible in the pseudo-tetragonal *ac* plane. Several crystals were checked along the [0 1 0] zone axis by HREM and by their Fourier transforms (FT), which corresponds to the conventional diffraction image. In the high-resolution micrographs of the majority of the crystals examined several domains with different orientations were observed. It is not clear whether this is a consequence of the preparation (grinding) of the crystals or a feature of original crystal growth. As a consequence, it is necessary to choose very small, highly ordered parts of the HREM image for a distinct imaging of satellite reflections for the FT. This, in turn, leads to low contrasts and poor intensities because of the small number of scattering centers.

The domain structure of the material can be seen in Figure 1 (top). The corresponding Fourier transform, depicted in the bottom part of Figure 1, shows a set of Bragg reflections, indicating an almost quadratic mesh with lattice parameters of 4.30 and 4.31 Å. These data match quite well with those obtained from X-ray investigations (cf. Table 1). However, satellite intensities, indicated by arrows, are hardly visible in the FT.

In the top part of Figure 2, the reconstructed phase image of an electron hologram of $LaSeTe_2$ is depicted. The FT of an electron hologram originally contains the central band, sometimes called auto correlation function, which corresponds to the conventional diffraction pattern, and two sidebands, which contain the phase information of the complex image wave. After masking out the central band and one sideband, the complex image wave is obtained by inverse FT of the remaining sideband. The FT of this reconstructed phase image of the electron hologram, depicted in the bottom part of Figure 2, clearly shows the Bragg reflections and two first-order satellite reflections, indicated by arrows. These main reflections and satellites are used to rebuild an image of the superstructure in direct space (Figure 3). The striped structure observed in Figure 3 indicates the orientation and width of the modulation wave of approximately 15 Å.

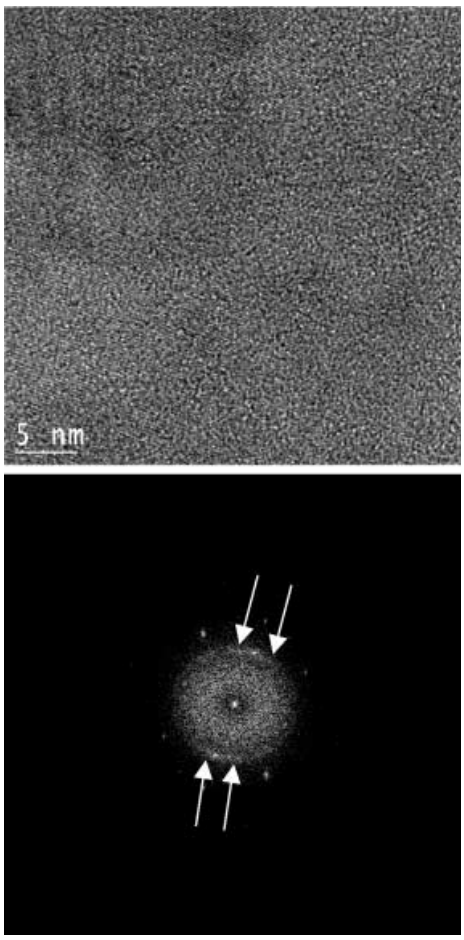

Figure 1. High-resolution micrograph (top) with its Fourier transform (bottom) showing weak satellite intensities (marked with white arrows) due to the occurrence of the superstructure.

X-ray structure refinement: Complete X-ray data sets at three different temperatures (173, 293, and 373 K) were collected for one suitable single crystal. Assuming isotypic average structures for $PrSeTe_2$ and $LaSeTe_2$ at room temperature,[7] a conventional three-dimensional starting model in space group *Cmcm* is easily available and the corresponding refinement converges to $wR_2 = 0.044$ for 19 parameters and 361 reflections (data set recorded at 173 K). However, some reflections which should be systematically absent due to the extinction conditions of this space group are observed with $I > 3\sigma I$ (see below).

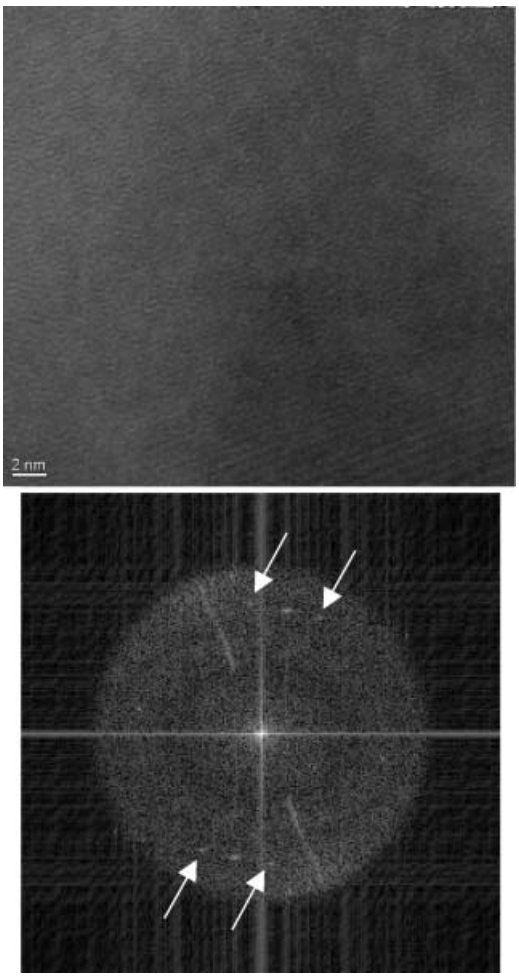

Figure 2. Reconstructed phase image of the electron hologram (top) and its power spectrum (FT, bottom) of the phase image with satellite reflections indicated by white arrows.

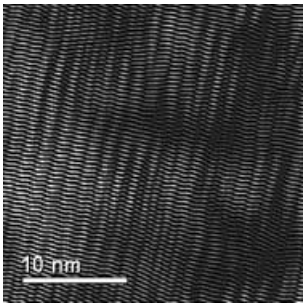

Figure 3. Recalculated image of the power spectrum of the phase image. Only one set of main reflections and its satellites were chosen in order to rebuild the superstructure. Evidently, a striped structure appears, indicating the orientation and width of the superstructure to be about 15 Å.

The satellites obey the superspace reflection condition $0klm$, $m=2n$, indicating the presence of a superspace glide plane perpendicular to the a axis. The modulation vector is $\mathbf{q}=\gamma\mathbf{c}^*$ with $\gamma=0.288$. On this basis, the 3+1-dimensional superspace group was assigned as $Cmcm(00\gamma)s00$ (No. 63.2) according to the standard setting of the International Tables for Crystallography, Part C.[9]

If the general positional atomic modulation function M is given as a sum of harmonic functions, $M_x(v)$ can be expressed as Equation (1):

$$M_x(v) = \sum_{n=1}^{m} S_{nx}\sin(2\pi nv) + C_{nx}\cos(2\pi nv) \quad (1)$$

Similar expressions are obtained for $M_y(v)$and $M_z(v)$. The symmetry restrictions generated by the site symmetry common to all atoms reduces the first harmonic terms ($n=1$) to that given in Equation (2):

$$M_x(v) = S_{nx}\sin(2\pi nv) \;\; M_y(v) = M_z(v) = 0 \quad (2)$$

It is then easy to generate an initial phasing model for the modulation by introducing small amplitude waves and trying all possible combinations of signs of S_{1x} for the different atoms. Since it was expected that the main contribution to the modulation would come from the Te atoms, the number of combinations could be reduced to four possibilities that are equivalent pairs. The proper choice turned out to be that of using opposite signs for S_{1x}(Te(1)) and S_{1x}(Te(2)). After making this choice, refinement proceeded smoothly. Because of the lack of higher order satellites with intensities above the detection threshold, it was deemed prudent not to introduce higher order harmonics for the description of the modulated behavior. In the final stages of the refinement, modulation waves for the lanthanum and selenium atoms, as well as modulation waves for the displacement parameters of all atoms were introduced. This led to a considerable drop in the R values for the satellite reflections, despite the small modulation of the displacement parameters. The structure model, however, yielded four fairly high residual electron density peaks (up to 5 e $Å^{-3}$) close to the positions of all four atoms in the refinement. This was determined to be a consequence of twinning of the crystal, the twin symmetry element being the mirror plane in $(\bar{1}01)$. The twin refinement converged to the residuals given in Table 1 with a twin fraction of 0.11(2); the subsequent difference Fourier map was featureless (cf. Table 1). The twinning explains the appearance of reflections that should be systematically absent. Because of the comparatively small scattering contribution of the second individual, not many satellites with intensities above the detection threshold are observed for this twin component. The refinements for the data sets collected at 293 and 373 K yielded comparable results and the resulting structure models exhibit only minor differences in the displacement parameters and the dislocation of the Te atoms (cf. Tables 1 and 2). The following structure description is based on the results of the low-temperature data collection (173 K). Information concerning crystallography, data collection, and structure refinement for all three data collections and refinements is listed in Table 1. The results of the refinement calculations are given in Table 2, interatomic distances and angles in Table 3.[10]

Structure description and discussion: Figure 4 shows the average structure of $LaSeTe_2$; the close relationship to the

Table 1. Crystallographic and refinement data for $LaSeTe_2$.

	$LaSeTe_2$ at 173 K	$LaSeTe_2$ at 293 K	$LaSeTe_2$ at 373 K
superspace group	$Cmcm(00\gamma)$s00 (No. 63.2)	$Cmcm(00\gamma)$s00 (No. 63.2)	$Cmcm(00\gamma)$s00 (No. 63.2)
a [Å]	4.295(1)	4.297(1)	4.309(1)
b [Å]	25.371(4)	25.408(4)	25.481(6)
c [Å]	4.306(1)	4.309(1)	4.321(1)
V [Å^3]	469.2(1)	470.4(1)	474.4(2)
γ [°]	0.288	0.288	0.288
ρ_{calcd} [g cm^{-3}]	6.69	6.66	6.61
μ [mm^{-1}]	28. 8	28.7	28.5
θ range [°]	3.2–28.1	3.2–28.0	3.2–29.3
reflections measured	5527	8289	6144
independent reflections	854	801	959
observed reflections [$I>3\sigma(I)$]	536	459	560
main reflections	356	334	397
observed reflections [$I>3\sigma(I)$]	351	323	388
satellites reflections	439	467	562
observed reflections [$I>3\sigma(I)$]	180	136	172
R_{int}/R_{sigma}	0.0362/0.005	0.039/0.009	0.051/0.008
weighting scheme	$w=1/[\sigma^2(I)+(0.0016(I^2)]$	$w=1/[\sigma^2(I)+(0.0016(I^2)]$	$w=1/[\sigma^2(I)+(0.0016(I^2)]$
min/max transmission	0.069/0.761	0.124/0.795	0.135/0.796
exctinction parameter residuals	0.10(1)	0.04(2)	0.20(2)
main reflections and satellites			
R_1/wR_2 ($I>3\sigma$); R_1/wR_2 (all I)	0.018/0.058; 0.036/0.070	0.027/0.076; 0.048/0.087	0.022/0.064; 0.046/0.074
main reflections only			
$R_1/wR_2(I>3\sigma)$; R_1/wR_2(all I)	0.016/0.056; 0.017/0.057	0.024/0.070; 0.025/0.071	0.019/0.060; 0.020/0.060
satellites only			
$R_1/wR_2(I>3\sigma)$; R_1/wR_2(all I)	0.037/0.069; 0.180/0.119	0.056/0.121; 0.238/0.177	0.053/0.095; 0.236/0.151
gooF ($I>3\sigma$)/(all I)	1.13/1.21	1.32/1.56	1.13/1.28
largest diff. peak/hole [e Å^{-3}]	1.50/−1.62	2.96/−3.06	1.75/−1.97

Table 2. Atomic coordinates, displacement parameter U_{eq} (Å$^2\times10^4$) and Fourier coefficient S_{1x} of the modulation function for $LaSeTe_2$.

		173 K				293 K			373 K		
atom	x	y	z	U_{eq}	S_{1x}	y	U_{eq}	S_{1x}	y	U_{eq}	S_{1x}
La	0	0.1766(1)	1/4	49(1)	0.0059(2)	0.1767(1)	59(2)	0.0051(2)	0.1767(1)	98(1)	0.0051(2)
Se	0	0.2968(1)	1/4	49(1)	0.0008(3)	0.2967(1)	60(2)	0.0008(4)	0.2966(1)	100(1)	0.0005(3)
Te(1)	0	-0.0715(1)	1/4	65(3)	−0.0224(3)	−0.0717(1)	85(2)	−0.0195(5)	−0.0716(1)	129(1)	−0.0198(4)
Te(2)	0	0.5718(1)	1/4	68(3)	0.0198(3)	0.5718(1)	86(2)	0.0175(5)	0.5718(1)	132(1)	0.0160(4)

U_{eq} is defined as 1/3 of the trace of the orthogonalized U_{ij} tensors.

Table 3. Average, minimum, and maximum interatomic distances [Å] and angles [°] for $LaSeTe_2$ at 173 K.

	av	min	max	max−min
La–Se	3.047(1)	3.047(1)	3.047(1)	0
La–Se	3.116(1)	3.101(1)	3.132(1)	0.031
La–Se	3.117(1)	3.101(1)	3.133(1)	0.032
La–Se	3.116(1)	3.101(1)	3.132(1)	0.031
La–Se	3.116(1)	3.101(1)	3.133(1)	0.032
La–Te(1)	3.428(1)	3.427(1)	3.429(1)	0.002
La–Te(1)	3.428(1)	3.427(1)	3.429(1)	0.002
La–Te(2)	3.418(1)	3.382(1)	3.457(1)	0.075
La–Te(2)	3.421(1)	3.382(1)	3.457(1)	0.075
Se–Te(2)	3.970(1)	3.970(1)	3.971(1)	0.001
Se–Te(2)	3.970(1)	3.970(1)	3.971(1)	0.001
Te(1)–Te(2)	3.043(1)	2.934(1)	3.155(1)	0.221
Te(1)–Te(2)	3.036(1)	2.930(1)	3.160(1)	0.230
Te(1)–Te(2)	3.044(1)	2.934(1)	3.155(1)	0.221
Te(1)–Te(2)	3.052(1)	2.923(1)	3.160(1)	0.237
∢Te-Te-Te	89.98(3)	86.44(4)	94.08(5)	7.64

$NdTe_3$ type is immediately apparent. The structure consists of puckered double layers of lanthanum and selenium atoms that are separated by two square-planar layers of tellurium atoms.

Lanthanum is surrounded by four tellurium (3.42–3.43 Å) and five selenium atoms (3.05–3.12 Å) forming a monocapped tetragonal antiprism. The selenium atom is coordinated by five lanthanum atoms in a square-pyramidal manner. The La–Se distances in the tetragonal base plane are approximately 3.11 Å, while the apical lanthanum atom is slightly closer (3.05 Å). The shortest Se–Te distances of about 3.97 Å are too large to be considered as bonding.

In the average structure, every tellurium atom is surrounded by four other tellurium atoms in a square-planar fashion at distances of 3.04 Å (Te–Te intralayer distance). These distances are only 11% longer than the sum of the covalent radii (2.74 Å) and fall within the typical range for bonding involving hypervalent tellurium atoms.[11] The coordination sphere is completed by two lanthanum atoms at distances of 3.42 Å.

The modulation mainly affects the tellurium positions and thus primarily alters the

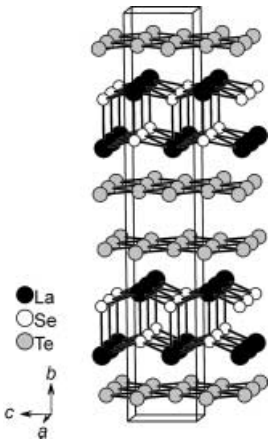

Figure 4. Average structure of $LaSeTe_2$; projection approx. along [100]; La: black circles, Se: open circles, Te: grey circles.

distances and angles within the [Te] layer. The slight sinusoidal modulation of the Te atoms can be visualized by the section of the Fourier maps along the modulation direction (Figure 5). The Te–Te distances vary between 2.92 and

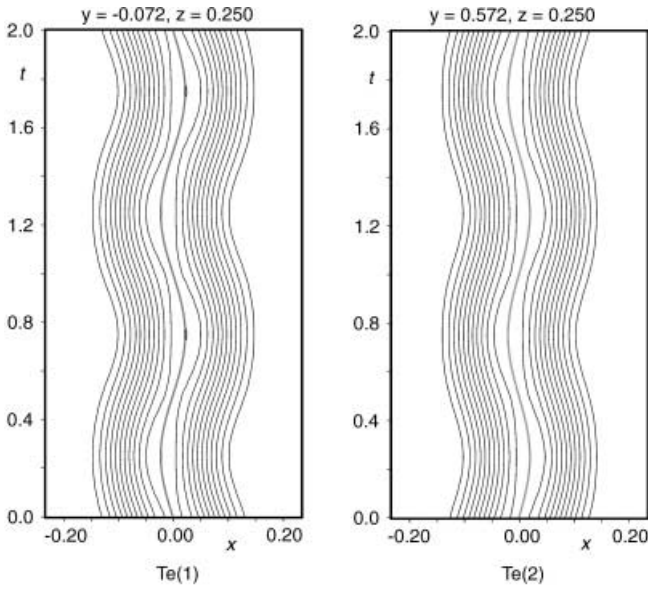

Figure 5. Fourier map plotted along the modulation direction (t); the calculated position of the Te atoms is given by the central grey line; only positive contour lines are given; one contour line per 20 e Å^{-3}.

3.16 Å, illustrating the tendency to form oligomeric Te_m^{n-} ions. The definition of a maximum Te–Te bonding distance is somewhat arbitrary, but if we consider only distances less than 3.00 Å, the [Te] layer can be described as containing "V-shaped" trimers and "N-shaped" tetramers, as well as heptamers resulting from the connection of one trimer and one tetramer (Figure 6, left). Distorted Te nets containing "V-shaped" trimers along with other tellurium entities are found in the modulated structures of $K_{1/3}Ba_{2/3}AgTe_2$, $RbUSb_{0.33}Te_6$, and $K_{0.65}Ag_2Eu_{1.35}Te_4$[12,1] (isolated Te_3^{2-} trimers are, of course, frequently found, e.g., in the structures of A_2Te_3 (A = alkali metal)[13]). If we take Te–Te distances of up to 3.04 Å (i.e., the Te–Te distance in the undistorted net of the average structure) into account, these oligomeric entities are then interconnected to give one-dimensional infinite chains (Figure 6, right), which show some similarities to the one-dimensional Te_3^{2-} chains in the structure of Tl_2Te_3 and the distorted Te net in $K_{2.5}Ag_{4.5}Ce_2Te_9$.[14,1]

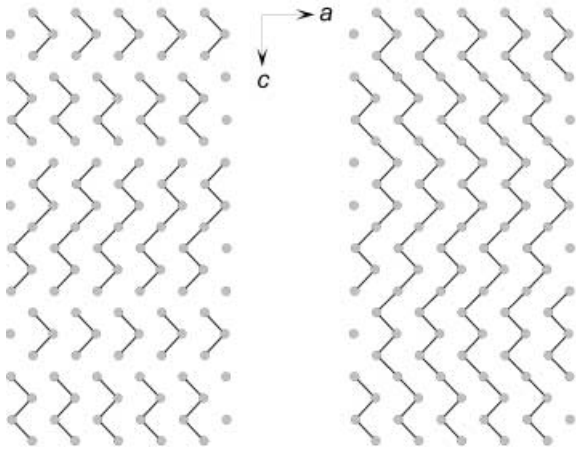

Figure 6. Projection on the [Te] net of the modulated structure of $LaSeTe_2$. Te–Te distances up to 3.0 Å (left) and up to 3.04 (right) Å are indicated as bonds.

Since S_{1x}(Te(1)) and S_{1x}(Te(2)) are of opposite sign and of similar amplitudes, the overall coordination of the lanthanum atoms is not much influenced by the modulation. The bond valence sum for La changes only slightly over one modulation period and shows almost no noticeable differences compared to that in the unmodulated structure.[15] The dislocations of the lanthanum and especially the selenium atom are so small that effective changes in their coordination geometry can be neglected.

A simple electron count according to the Zintl–Klemm concept shows that if we consider lanthanum as La^{3+} and selenium as Se^{2-}, each Te atom has to carry a formal charge of −0.5 giving the structural formula $[LaSe]^{1+}[Te]^{0.5-}[Te]^{0.5-}$. As has been stated previously, covalently bonded 4^4 nets of chalcogen atoms with an electron count of six or more valence electrons per atom are prone to distortion due to a Peierls type instability.[16] Different types of distortions have been observed in compounds of this type. In the stoichiometric rare-earth dichalcogenides $LnE_{2.0}$ (with E = S, Se, Te), which have a larger amount of excess electrons per E atom in the square layer (formally E^{1-}), a localization of electrons in oligomeric anionic units, mainly in E_2^{2-} dimers, turns out to be the most favorable.[17] Most of the rare-earth diselenides and ditellurides are semiconductors, but metallic behavior was reported, for example, for $LaTe_2$ and $CeTe_2$.[17k,f] The lanthanide chalcogenides $LnE_{2-\delta}$ ($0 < \delta < 0.4$) contain chalcogen vacancies, as well as monomeric and oligomeric anionic entities in their defective [E] layer, and they are usually semiconducting (cf. ref. [18]). Lanthanide tritellurides $LnTe_3$ and dilanthanide pentatellurides Ln_2Te_5 were found to host charge-density waves. The modulations of the compounds $LnTe_3$ and the related dichalcogenides $LaSe_2$ and $LaTe_2$ have been discussed in terms of Fermi surface nesting,[4,19,20] and the direction of the distortions can be deduced from the nesting vectors. Nevertheless, $SmTe_3$ and Sm_2Te_5 still exhibit metallic conductivity parallel to the [Te] layers in their modulated state, indicating that only a partial gap opens over the Fermi surface.[4] Semimetallic or semiconducting behavior is also found for some ternary and quaternary rare-earth polytellurides.[1] DFT (density functional theory) calculations of the band structure were in a first step carried out based on the average structure of $LaSeTe_2$, suggesting that the compound should be a poor metal in its non-modulated state. The complete density of states (DOS) is given in the right-hand part of Figure 7. A non-zero DOS at the Fermi level suggests metallic behavior for the non-modulated phase of $LaSeTe_2$. The left-hand part of this figure shows the band structure; bands with Te contributions are emphasized. As can be seen from the figure, states at the Fermi level have mainly Te $5p_x$ and $5p_y$ contributions, in-

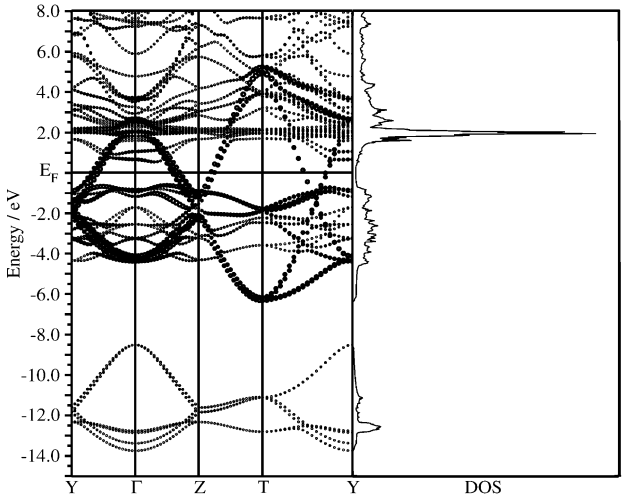

Figure 7. Left: Band structure of the average structure of $LaSeTe_2$, states with Te contributions are given as fat bands. Right: total density of states (DOS) of the average structure; $\Gamma=(0, 0, 0)$, $Y=(^1/_2, 0,0)$, $Z=(0, 0, ^1/_2)$, $T=(^1/_2, 0, ^1/_2)$.

dicating that the metallic conductivity should essentially be related to these bands. In the Te–Te crystal orbital overlap population curve based on extended Hückel calculations of

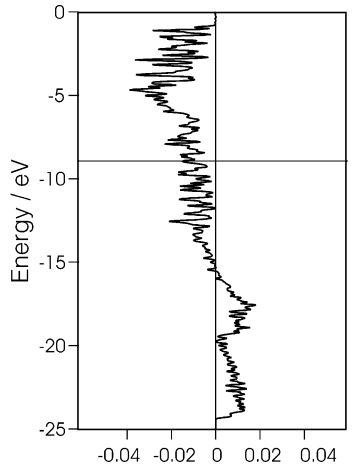

Figure 8. Plot of the crystal orbital overlap population for the Te–Te interactions.

the average structure (Figure 8), the electron excess discussed above is clearly visible in the occupation of antibonding states below the Fermi level. A second calculation was performed at the extended Hückel level, with the atoms of the Te nets arranged in a sevenfold supercell (a, b, $7c$; space group $C2/c$) as a commensurate approximation of the modulated structure (Figure 9). Although the modulation leads to an alteration of the Te–Te distances of less than five percent, a fairly large change in the dispersion of the bands along the modulation direction ($\Gamma\rightarrow Z$) results. Furthermore, the top of the highest occupied band and the

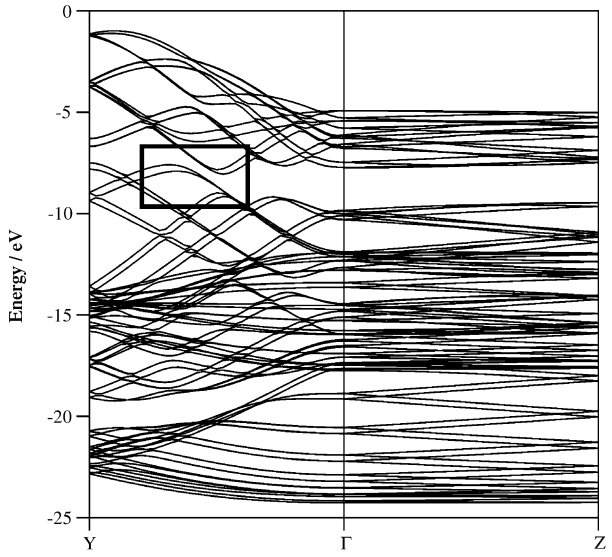

Figure 9. Band structure of the modulated phase of $LaSeTe_2$ (commensurate approximation in a sevenfold supercell); the opening of the indirect band gap is emphasized with the box; $\Gamma=(0, 0, 0)$, $Y=(^1/_2, 0,0)$, $Z=(0, 0, ^1/_2)$.

bottom of the lowest unoccupied band are clearly shifted away from each other along the $\Gamma\rightarrow Y$ direction, and an indirect band gap opens as a consequence. According to these results the modulated phase of $LaSeTe_2$ should be considered to be a semimetal, consistent with the description as a compound with imperfect Fermi surface nesting.

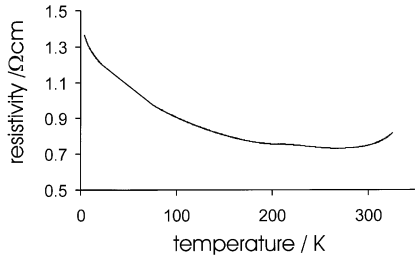

Figure 10. Plot of the resistivity versus temperature.

The temperature dependence of the electrical resistivity of $LaSeTe_2$ as a powder pellet is given in Figure 10. The negative slope of the resistivity between 4 K and room temperature indicates semiconducting or semimetallic behavior, in accordance with the calculation based on the commensurate approximation of the modulated structure. The resistivity data suggests that a change in the transport properties occurs slightly above room temperature; this should be correlated with a transition into a non-modulated state. At 373 K, however, satellite reflections are still present. The displacement parameters of all atoms increase with increasing temperature, while the dislocations of the Te atoms decrease (cf. Table 2); this can be taken as a further hint for a transition to a non-modulated state. The modulation vector **q** does not change noticeably between 173 and 373 K.

Experimental Section

Preparation: All preparational steps were carried out under dried argon (Messer-Griesheim, Krefeld, Germany, 99.96 %). Stoichiometric amounts of lanthanum (Chempur, Karlsruhe, Germany, powder, 99.9 %), selenium (Strem, Kehl, Germany, powder, 99.99 %), and tellurium (Fluka, Germany, pieces, 99.999 %) were loaded into silica ampoules together with a tenfold excess of a 1:1 mixture of LiCl and RbCl as flux material. LiCl and RbCl (both: Merck, Darmstadt, Germany, 99+ %) were dried by heating under dynamic vacuum prior to use. The ampoules were sealed under vacuum and placed into an oven. The mixtures were heated to 970 K at 10 $K\,min^{-1}$ and kept at this temperature for 7 days. The ampoules were then cooled to room temperature (0.03 $K\,min^{-1}$) and opened. The flux was removed with water, and the crystals were washed with ethanol and then dried in air. Thin, shiny gold platelets with sizes up to 0.2 mm grew under these conditions.

Analysis: EDX analyses (Zeiss Digital Scanning Microscope 982 Gemini with Noram Voyager analytic unit) showed no detectable impurities of flux or other element in the crystals and confirmed the composition of the compound.

Electron microscopy: HREM and electron holography were carried out at the Triebenberg Special Laboratory (Dresden) with a Philips CM200 FEG\SuperTwin-Lorentz Microscope. The microscope was equipped with a field emission gun operating with an accelerating voltage of 200 kV. Holograms were taken at a magnification of 868.000×, with hologram fringe spacings of 1.6 Å (corresponding to a nominal resolution of 3.2 Å) and a biprism voltage of 230 V. Micrographs and holograms were recorded with a 1×1 k CCD-camera and were fed into the computer for on-line processing and reconstruction in nearly real-time mode. The holograms were evaluated by the software Digital Micrograph 3.3.1 (Gatan). In the holographic experiments, the incoming wave is separated into an object and a reference wave. The reference wave runs through vacuum and is not influenced by the object. A biprism superimposes both waves to produce the interference pattern, the electron hologram. The digitalized hologram was processed in the computer, where the phase and the amplitude of the recorded wave was reconstructed.

For these investigations, the crystals were ground under ethanol. Some drops of this suspension were placed on a copper grid coated with a holey carbon foil. The ethanol was then allowed to evaporate. Due to their laminar structure, the crystals cleave quite easily to give very thin platelets, some being transparent to the electron beam. In addition, this preparation method results in a preferred orientation of the platelets perpendicular to [0 1 0], the desired orientation for both electron diffraction and holography. The samples were then coated with a carbon layer to prevent radiation damage and charging. Due to the mechanical strain during grinding, distortion and translocation of atomic layers (e.g., a slipping of the [Te] layers) can easily occur, leading to stacking faults in the crystals.

X-ray investigations: Several crystals of $LaSeTe_2$ were mounted on quartz capillaries and precession images were recorded. No satellite reflections were observed in zero-level layer photographs, but after long exposures satellites did appear in the upper-level records *h1l* near main reflections with $L=2n$, and *h2l* near main reflections with $L=2n+1$, indicating a one-dimensional incommensurate modulation of the structure. Subsequently, a suitable crystal of dimensions $0.02\times0.06\times0.15$ mm^3 was mounted on a diffractometer (STOE IPDS-II, $Mo_{K\alpha}$ radiation, graphite monochromator) equipped with a N_2-cryosystem (Cryostream controller 700, Oxford, UK) for temperature control, and complete data sets including first-order satellites were recorded at 173, 293, and 373 K. Absorption corrections of the 3+1-dimensional data sets were performed using the program JANA2000;[21] the shape of the crystal was determined and refined based on average structure data using the STOE software package.[22] The full-matrix least-squares refinements of both the average and modulated structures were carried out with JANA2000 against F^2. Extinction effects were corrected according to Becker and Coppens.[23]

Calculations: DFT (density functional theory) calculations were performed with the WIEN97 code with the LAPW (linearized augmented plane wave) method.[24] The muffin-tin radii were chosen to be 2.5 au for La, Te, and Se. RKMAX and GMAX were taken to be 9 and 13 au^{-1}, respectively. The generalized gradient approximation functional PBE-GGA was used as the exchange-correlation functional.[25] The Brillouin zone integration was performed by means of a tetrahedron method with 155 inequivalent k points corresponding to 1000 k points throughout the whole Brillouin zone within the SCF cycles.[26] For calculation of the density of states (DOS) 392 inequivalent k point (3000 k points in the Brillouin zone) were used. The extended Hückel calculations were performed by using the program YAeHMOP with the following parameters: orbital energies H_{ij} [eV] (coefficient $\zeta1$): Se: 4s −20.50 (2.44), 6p −14.40 (2.07); Te: 5s −20.80 (2.51), 5p −14.80 (2.16); La 6s −7.67 (2.14), 6p −5.01 (2.08), 5d −8.21 (3.78); double ζ-functions for La: 0.7765, 1.381, 0.4586.[27]

Electrical transport properties: Since the single crystals obtained by flux reactions were too small for electrical contacting, the resistivity was measured on powder pellets using van der Pauw's method.[28]

Representation of the crystal structure: Figures displaying parts of the crystal structure were generated with DIAMOND.[29]

Acknowledgement

The authors thank Prof. Dr. H. Lichte and Dr. M. Lehmann, (TU Dresden) for the support of the HREM and holographic experiments, Dr. W. Schnelle (Max-Planck-Institute for Chemical Physics of Solids, Dresden) for the resistivity measurements, Mrs. E. Kern (TU Dresden) for the EDX analyses, and Dr. A. Mills (TU Dresden) for a critical review of the manuscript. Financial support by the Deutsche Forschungsgemeinschaft is gratefully acknowledged.

[1] R. Patschke, M. G. Kanatzidis, *Phys. Chem. Chem. Phys.* **2002**, *4*, 3266.
[2] P. Böttcher, Th. Doert, H. Arnold, R. Tamazyan, *Z. Kristallogr.* **2000**, *215*, 246.
[3] a) W. Lin, H. Steinfink, E. J. Weiss, *Inorg. Chem.* **1965**, *4*, 877; b) B. K. Norling, H. Steinfink, *Inorg. Chem.* **1966**, *5*, 1488; c) M.-P. Pardo, J. Flahaut, *Bull. Soc. Chim. Fr.* **1967**, *10*, 3658.
[4] E. DiMasi, B. Foran, M. C. Aronson, S. Lee, *Chem. Mater.* **1994**, *6*, 1867.
[5] E. DiMasi, M. C. Aronson, J. F. Mansfield, B. Foran, S. Lee, *Phys. Rev. B* **1995**, *52*, 14516.
[6] G.-H. Gweon, J. D. Denlinger, J. A. Clack, J. W. Allen, C. G. Olson, E. DiMasi, M. C. Aronson, B. Foran, S. Lee, *Phys. Rev. Lett.* **1998**, *81*, 886.
[7] B. P. T. Fokwa, Th. Doert, P. Simon, T. Söhnel, P. Böttcher, *Z. Anorg. Allg. Chem.* **2002**, *628*, 2612.
[8] a) H. Lichte, *Philos. Trans. R. Soc. London Ser. A* **2002**, *360*, 897; b) M. Lehmann, H. Lichte, D. Geiger, G. Lang, E. Schweda, *Mater. Charact.* **1999**, *42*, 249; c) P. A Midgley, *Micron* **2000**, *32*, 167; d) E. Völkl, L. F. Allard, D. C. Joy: *Introduction to Electron Holography*, Kluwer Academic, Plenum, New York, **1999**.
[9] *International Tables for Crystallography, Part C* (Ed.: A. J. C. Wilson), Kluwer Academic, Dordrecht, **1995**.
[10] Further details on the crystal structure investigations can be obtained from the Fachinformationzentrum Karlsruhe, 76344 Eggenstein-Leopoldshafen (fax: (0049)7247-808-666 e-mail: crysdata@fiz.karlsruhe.de), on quoting the depository numbers CSD 413173 (173 K), CSD 413172 (293 K), and CSD 413171 (373 K).
[11] a) P. Böttcher, U. Kretschmann, *Z. anorg. allg. Chem.* **1982**, *491*, 39; b) P. Böttcher, U. Kretschmann, *J. Less-Common Met.* **1983**, *95*, 81; c) P. Böttcher, R. Keller, *J. Less-Common Met.* **1985**, *109*, 311; d) W. S. Sheldrick, M. Wachhold, *Angew. Chem.* **1997**, *109*, 214; *Angew. Chem. Int. Ed. Engl.* **1997**, *36*, 206.
[12] a) X. Zhang, J. Li, B. Foran, S. Lee, H.-G. Guo, T. Hogan, C. R. Cannewurf, M. G. Kanatzidis, *J. Am. Chem. Soc.* **1995**, *117*, 10513; b) K.-S. Choi, M. G. Kanatzidis, *J. Solid State Chem.* **2001**, *161*, 17.
[13] a) P. Böttcher, *Z. Anorg. Allg. Chem.* **1977**, *432*, 167; b) B. Eisenmann, H. Schäfer, *Angew. Chem.* **1978**, *90*, 731; *Angew. Chem. Int. Ed. Engl.* **1978**, *17*, 684; c) P. Böttcher, *Z. Anorg. Allg. Chem.* **1980**, *461*, 13.

[14] Th. Doert, P. Böttcher, R. Cardoso-Gil, *Z. Anorg. Allg. Chem.* **1999**, *625*, 2160.
[15] I. D. Brown, D. Altermatt, *Acta Crystallogr. Sect. B* **1985**, *41*, 625.
[16] a) W. Tremel, R. Hoffmann, *J. Am. Chem. Soc.* **1987**, *109*, 124; b) R. Hoffmann, *Solids and Surfaces*, VCH, New York, **1988**; c) G. A. Papoian, R. Hoffmann, *Angew. Chem.* **2000**, *112*, 2500; *Angew. Chem. Int. Ed.* **2000**, *39*, 2408.
[17] a) J. Dugué, D. Carré, M. Guittard, *Acta Crystallogr. Sect. B* **1978**, *34*, 403; b) S. Benazeth, D. Carré, P. Laruelle, *Acta Crystallogr. Sect. B* **1982**, *38*, 33; c) S. Benazeth, , D. Carré, P. Laruelle, *Acta Crystallogr. Sect. B* **1982**, *38*, 37; d) R. Tamazyan, H. Arnold, V. Molchanov, G. Kuzmicheva, I. G. Vasileva, *Z. Kristallogr.* **2000** ,*215*, 272; e) K. Stöwe, *J. Alloys Compd.* **2000**, *307*, 101; f) K. Stöwe, F. R. Wagner, *J. Solid State Chem.* **2000**, *149*, 155.
[18] a) E. Dashjav, Ph.D. Thesis, Dresden (Germany) **2001**; b) K. Stöwe, *Z. Kristallogr.* **2001** ,*216*, 215.
[19] A. Kikuchi, *J. Phys. Soc. Jpn.* **1998**, *67*, 1308.
[20] B. Foran, S. Lee, *J. Am. Chem. Soc.* **1996**, *118*, 9193.
[21] JANA2000, Crystallographic Computing System, V. Petricek, M. Dusek, Prague, **2002**.
[22] X-RED: Programm for Data Reduction and Absorption Correction, STOE & Cie., Darmstadt, **2001**; X-SHAPE: Crystal Optimisation for Numerical Absorption Correction, STOE & Cie., Darmstadt, **1999**.
[23] P. J. Becker, P. Coppens, *Acta Crystallogr. Sect. A* **1974**, *30*, 129; P. J. Becker, P. Coppens, *Acta Crystallogr. Sect. A* **1974**, *30*, 147.
[24] P. Blaha, K. Schwarz, J. Luitz, WIEN97, A Full Potential Linearized Augumented Plane Wave Package for Calculating Crystal Properties, Vienna University of Technology, Vienna (Austria), **1999**.
[25] J. P. Perdew, S. Burke, M. Ernzehof, *Phys. Rev. Lett.* **1996**, *77*, 3865.
[26] P. E. Blöchl, O. Jepsen, O. K. Andersen, *Phys. Rev. B* **1994**, *49*, 16223.
[27] G. Landrum, YAeHMOP, Yet Another extended Hückel Molecular Orbital Package, Cornell University, Ithaka (USA), **1997** (http://yaehmop.sourceforge.net/).
[28] L. J. van der Pauw, *Philips Res. Rep.* **1958**, *13*, 1.
[29] G. Bergerhoff, DIAMOND, Visual Crystal Information System, Bonn, **1999**.

Received: May 16, 2003 [F5148]